A New Approach to Characterizing Sorption in Materials with Flexible Micropores

Roberto Anedda,[†] Dmitriy V. Soldatov,[‡] Igor L. Moudrakovski,*[,§] Mariano Casu,[†] and John A. Ripmeester[§]

Department of Chemical Sciences, University of Cagliari, Cittadella Universitaria di Monserrato, S.S. 554 Bivio Sestu, 09042 Monserrato (CA), Italy, Department of Chemistry, University of Guelph, 50 Stone Road East, Guelph, Ontario N1G 2W1, Canada, and Steacie Institute for Molecular Sciences, National Research Council, 100 Sussex Drive, Ottawa, Ontario K1A 0R6, Canada

Received October 22, 2007. Accepted February 25, 2008

Microporous dipeptides, also known as organic zeolites or biozeolites, as examples of small-pore peptide nanotubes provide a convenient set of materials for developing a systematic approach based on ^{129}Xe NMR spectroscopy for the derivation of thermodynamic and molecular scale information on temperature dependent pore filling. The sorption of xenon in the isolated 1D chiral nanochannels of eight microporous dipeptides Ala-Val (AV), Val-Ala (VA), Leu-Ser (LS), Ala-Ile (AI), Val-Val (VV), Ile-Ala (IA), Ile-Val (IV), Val-Ile (VI) (all LL isomers) was monitored in situ with continuous-flow ^{129}Xe NMR spectroscopy over a temperature range of 173−343 K. The materials all showed strongly anisotropic signals, with isotropic chemical shift changing from 95 to 281 ppm depending on the dipeptide used and/or temperature. The isosteric heats of sorption (q_{st}) and entropy factors were determined from two independent models. The sorption process was complicated by reversible phase transformations of some dipeptides and irreversible changes due to aging of samples, both of which may be of considerable importance in applications of soft materials. The interpretation of the line shapes and chemical shift anisotropy as a function of temperature provided information on the structure of the xenon-cavity complex and made it possible taking into account the helicity and flexibility of the nanochannels and the dynamics of xenon. The approach illustrates a powerful way of analyzing pore space in soft microporous materials, yielding a quantitative thermodynamic description of sorption and the characteristics of the pore space and sorption events that occur on molecular-scale level during pore filling.

Introduction

Microporous materials are the subject of extensive research because of the availability of well-defined void space with different sizes and shapes suitable for a variety of applications, such as molecular storage and nanoreservoirs for reaction.[1] Current and potential future applications of these materials include industrial catalysis, gas sensing and storage, isolation and stabilization of pharmaceuticals, biological molecules and reactive species, and various purification and separation technologies. Although most such materials currently used on an industrial scale are inorganic in nature, metal−organic and organic analogs (such as "organic zeolites"[2] and "organic clays"[3]) are thought to constitute the future generation of practically useful microporous solids.[2,4,5]

Microporous materials assembled from building blocks of which at least one is organic have a tremendous diversity: a near-infinite number of building blocks and modes of assembly make it possible to create a multitude of structural motifs, where chemical and structural modulations may be introduced in small increments over a wide range to create the desired property or function.[2,5] At the same time, many aspects in the design and utilization of these materials appear to be very complex and need adequately organized fundamental studies before these materials become able to compete with their inorganic predecessors.

The object of this study is the characterization of void space in flexible pore systems such as biozeolites, a new group of microporous materials based on peptides. In these materials, peptide nanotubes form as a result of the H-bonded helical assembly of dipeptide molecules in crystals[6–14] with

* Corresponding author. E-mail: Igor.Moudrakovski@nrc-cnrc.gc.ca.
[†] University of Cagliari.
[‡] University of Guelph.
[§] Steacie Institute for Molecular Sciences, National Research Council.

(1) Atwood, J. L.; Davies, J. E. D.; MacNicol, D. D.; Vögtle, F. *Comprehensive Supramolecular Chemistry*; Pergamon: Exeter, U.K., 1996, Vol. 7.
(2) Soldatov, D. V.; Ripmeester, J. A. *Stud. Surf. Sci. Catal.* **2005**, *156*, 37–54.
(3) Beatty, A. M.; Schneider, C. M.; Simpson, A. E.; Zaher, J. L. *CrystEngComm* **2002.**, *4*, 282–287, and refs 1−12 therein.
(4) Kitagawa, S.; Kondo, M. *Bull. Chem. Soc. Jpn.* **1998**, *71*, 1739–1753.
(5) Soldatov, D. V. *Stimuli-Responsive Supramolecular Solids: Functional Porous and Inclusion Materials* Urban, M. W., Ed.; ACS Symposium Series 912; American Chemical Society: Washington, D.C., 2005; Chapter 13, pp 214−231.
(6) Bong, D. T.; Clark, T. D.; Granja, J. R.; Ghadiri, M. R. *Angew. Chem., Int. Ed.* **2001**, *40*, 988–1011.
(7) Görbitz, C. H. *New J. Chem.* **2003**, *27*, 1789–1793.
(8) Soldatov, D. V.; Moudrakovski, I. L.; Grachev, E. V.; Ripmeester, J. A. *J. Am. Chem. Soc.* **2006**, *128*, 6737–6744.
(9) Görbitz, C. H. *Chem.−Eur. J.* **2007**, *13*, 1022–1031.
(10) Gorbitz, C. H.; Gundersen, E. *Acta Crystallogr., Sect. C* **1996**, *52*, 1764–1767.
(11) Gorbitz, C. H.; Nilsen, M.; Szeto, K.; Tangen, L. W. *Chem. Commun.* **2005**, 4288–4290.
(12) Gorbitz, C. H. *Chem. Eur. J.* **2001**, *7* (23), 5153–5159.

10.1021/cm8001805 CCC: $40.75 © 2008 American Chemical Society
Published on Web 04/22/2008

the formation of micropores resulting from combinations of various amino acids.[7,8] It seems to be a common pattern of oligopeptide applications that, taking into account their combinatorial diversity, could entirely revolutionize the domain of engineering microporous solids. Sorption studies have already revealed size-matching molecular recognition by the biozeolites[14] and the design of peptide sorbents that are highly selective to a particular guest will likely be possible within this diversity. Further advantages of biozeolites include their harmlessness, biocompatibility and environmental friendliness. On the other hand, the microporous dipeptides display not only similarities to inorganic sorbents, such as uniform micropore geometry, a highly ordered well-defined structure, and homogeneity of the bulk solid phase, but also some characteristic features of proteins: flexibility of the micropores, structural "softness", and the capability of easy structural transformations. In other words, the peptide-based micropores may be used as simple models of biological ion channels and transmembrane pores,[15] as well as to further a better understanding of inclusion in proteins, where the included species may induce significant changes in the conformation and tertiary/quaternary structure of the protein molecule. Although deformations of the porous framework induced by sorbate inclusion have been previously observed in some zeolites,[16] they represent a phenomenon that is still rare. The relevance of framework flexibility in modulating sorption properties and specificity of inorganic materials is quite evident.[17] On the other hand, the importance of understanding the role of protein flexibility in regulating catalytic enzymatic processes, and biological activity in general,[18] and the implication of these issues in the development of drug discovery[19] are well-recognized.

^{129}Xe NMR spectroscopy has proven to be an extremely sensitive and informative method for studying void spaces, both in porous materials and in proteins.[20–22] The development of continuous-flow techniques with hyperpolarized xenon nuclei have expanded the capabilities of the method dramatically and have made possible the rapid characterization of materials and other systems.[23–25]

Since the earliest ^{129}Xe NMR experiments on characterization of porous materials, a number of different theories have been proposed, aimed at finding a good correlation between the NMR parameters of the guest xenon atom probes (chemical shifts, line shapes, relaxation times) and the actual structure of the hosts. However, although high sensitivity of the easily polarizable xenon electronic cloud to its physical environment potentially provides plenty of information, the experimental NMR parameters are often influenced by a number of different concurrent contributions. Calculations based on Lennard−Jones potentials[26,27] demonstrated that, in fact, a single simple correlation between ^{129}Xe NMR chemical shift and void space is not expected and the chemical shift of xenon adsorbed in microporous materials is a complicated function of void space geometry, sorption energy, and temperature. Considerable progress has been made in the derivation of useful parameters for sorption from ^{129}Xe NMR spectroscopy of large pore sytems ($d \gtrsim 1$ nm). In those cases, the line shape is dominated by exchange and dynamics, and parameters pertaining to pore size, sorption energy, etc., can be derived using a simple model that uses the temperature dependence of the chemical shift.

Even though the relationship between shielding tensors and pore size and shape is well-understood for small pore systems, a general approach to the actual derivation of useful parameters from NMR spectroscopy has not been demonstrated. This study is aimed at the detailed characterization of sorption in the flexible channels of microporous dipeptides. In particular, we focus on the fundamental thermodynamic parameters and molecular-scale peculiarities of the sorption process and how these characteristics relate to the structure of the micropores. As demonstrated previously,[8] the pores are very flexible and the pore structure revealed in the crystal structure examination of an empty sorbent will not account for its sorption behavior as the pores become loaded with the guest species. For flexible pore systems, researchers must expect that the model obtained for the pore structure will depend very much on the characterization technique employed.

Experimental Section

Materials. Eight dipeptides (AV (Ala-Val), VA (Val-Ala), AI (Ala-Ile), LS (Leu-Ser), VV (Val-Val), IA (Ile-Ala), IV (Ile-Val), and VI (Val-Ile), Figure 1) were purchased from Bachem. LS had to be recrystallized and desolvated prior to preparation, as described previously.[8] Powdered samples for ^{129}Xe NMR analysis were prepared by grinding as-received materials followed by drying them overnight at 60 °C to remove the residual moisture. Such a soft treatment is sufficient, because the heating of the samples at 120 °C in a vacuum did not produce any appreciable mass loss that could be attributed to adsorbed water. In addition, the samples were purged with a continuous flow of the Xe−N_2−He gas mixture (BOC, Canada, volume composition Xe:N_2:He = 1:3:96) at room temperature for 10−15 min in the NMR probe before each NMR experiment. About 70 mg of each dipeptide was sufficient to obtain a good signal-to-noise ratio for all spectra.

To test the effect of Xe sorption on the dipeptides' frameworks by ^{13}C NMR, we also prepared sealed samples of all studied dipeptides with adsorbed Xe. These samples were made by evacuating the original dipeptides in a vacuum of 1×10^{-6} mbar

(13) Moudrakovski, I.; Soldatov, D. V.; Ripmeester, J. A.; Sears, D. N.; Jameson, C. J. *Proc. Natl. Acad. Sci. U.S.A.* **2004**, *101*, 17924–17929.
(14) Soldatov, D. V.; Moudrakovski, I. L.; Ripmeester, J. A. *Angew. Chem., Int. Ed.* **2004**, *43*, 6308–6311.
(15) Percec, V.; Dulcey, A. E.; Balagurusamy, V. S. K.; Miura, Y.; Smidrkal, J.; Peterca, M.; Nummelin, S.; Edlund, U.; Hudson, S. D.; Helney, P. A.; Duan, H.; Magonov, S. N.; Vinogradov, S. A. *Nature* **2004**, *430*, 764–768.
(16) Mentzen, B. F.; Gelin, P. *Mater. Res. Bull.* **1995**, *30*, 373–380.
(17) Kuznicki, S. M.; Bell, V. A.; Nair, S.; Hillhouse, H. W.; Jacubinas, R. M.; Braunbarth, C. M.; Toby, B. H.; Tsapatsis, M. *Nature* **2001**, *412*, 720–724.
(18) Zaccai, G. *Science* **2000**, *288*, 1604–1607.
(19) Teague, S. J. *Nat. Rev.* **2003**, *2*, 527–541.
(20) Ratcliffe, C. I. *Annu. Rep. NMR Spectrosc.* **1998**, *36*, 124–208.
(21) Goodson, B. M. *J. Magn. Reson.* **2001**, *155*, 157–216.
(22) Bonardet, J.; Fraissard, J.; Gedeon, A.; Springuel-Huet, M. *Catal. Rev. Sci. Eng.* **1999**, *41*, 115–225.
(23) Simonutti, R.; Bracco, S.; Comotti, A.; Mauri, M.; Sozzani, P. *Chem. Mater.* **2006**, *18* (19), 4651–4657.
(24) Sozzani, P.; Bracco, S.; Comotti, A.; Mauri, M.; Simonutti, R.; Valsesia, P. *Chem. Commun.* **2006**, 1921–1923.
(25) Baumer, D.; Brunner, E.; Blümler, P.; Zänker, P. P.; Spiess, H. W. *Angew. Chem., Int. Ed.* **2006**, *45*, 7282–7284.
(26) Ripmeester, J. A.; Ratcliffe, C. I. *J. Phys. Chem.* **1990**, *94*, 7652–7656.
(27) Cheung, T. T. P. *J. Phys. Chem.* **1995**, *99*, 7089–7095.

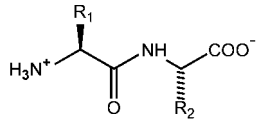

	R_1	R_2
AV	Methyl	iso-Propyl
VA	iso-Propyl	Methyl
AI	Methyl	sec-Butyl
VV	iso-Propyl	iso-Propyl
IA	sec-Butyl	Methyl
IV	sec-Butyl	iso-Propyl
VI	iso-Propyl	sec-Butyl
LS	iso-Butyl	Hydroxymethyl

Figure 1. Molecular structure of dipeptides studied.

at 120 °C for 12−15 h. After being cooled to room temperature, the samples were exposed to about 900−950 mbar of Xe gas, equilibrated for 1 h at room temperature, and then flame-sealed. A set of control samples without Xe was also prepared.

NMR Measurements. All ^{129}Xe NMR spectra were obtained on a Bruker AMX300 spectrometer operating at 83.013 MHz (magnetic field 7.05 T) using a customized probe from Morris Instruments. The majority of the experiments were performed using a continuous flow of hyperpolarized Xe gas, as described previously.[28] The flow rate was monitored using a Fathom Technologies flow controller (model GR-116 3-A-PV). The gas flow was set to 0.3 L/h in order to achieve a good signal-to-noise ratio and kept constant for each experiment. A solid-state spin−echo sequence was used to acquire all of the data[29] with 90° pulse length of 3 μs and 180° pulse of 6 μs. τ_1 and τ_2 delays were chosen as short as 100 μs and a recycle time of 1 s was used. The ^{13}C NMR experiments were performed on a Bruker Avance-200 instrument (magnetic fields of 4.7 T) and ^{13}C resonance frequencies of 50.3 MHz. Cross-polarization magic angle spinning (CP MAS) measurements on the sealed samples were performed using a Chemagnetic 7.5 mm Pencil probe. Optimized contact times of 1 ms and relaxation delays of 3 s were used.

The continuous flow of hyperpolarized (CF HP) Xe was delivered to the NMR coil through a 2 mm plastic tubing. The temperature in the probe was controlled using a Bruker BT1000 temperature controller with an accuracy of 0.1 K. The variable-temperature experiments were performed with decreasing temperature stepwise from 343 to 173 K. The sample was allowed to equilibrate at each temperature for 10 min before the corresponding spectrum was collected. The observed intensities, chemical shifts, and signal anisotropies were constant for the same dipeptide at a given temperature and they showed reproducible values over a series of repeated measurements. Also, the temperature-dependent changes upon heating and cooling were reversible.

The reported ^{129}Xe and ^{13}C chemical shifts were referenced to xenon gas, set to 0 ppm, and liquid tetramethylsilane (TMS), also set to 0 ppm. Analysis of the anisotropic lineshapes was performed using a simulation module of the Bruker Topspin 1.3 processing program. Integration of the signals was done using the Bruker processing program XWinNMR. The relative integral intensity of the signal (I) was calculated as the ratio of intensity from the signal of xenon residing in the nanochannels (I_{ch}) and the combined intensity of xenon in the gas phase and xenon adsorbed on the external particle surface and intercrystallite regions (I_{gas}).

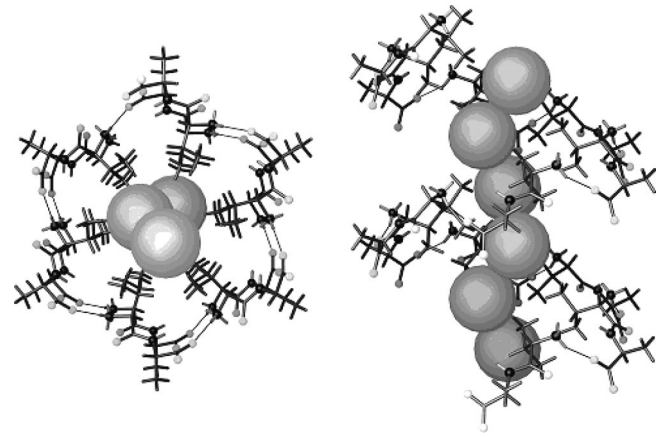

Figure 2. Fragment of the crystal structure of VA (hexagonal, space group $P6_1$) showing H-bonding helical assembly of the dipeptide molecules surrounding the channel: a view along the channel (left) and side view (right). Two translational periods are shown. N and O atoms are drawn as small black and white balls, respectively. H-bonds are designated with thin grey lines. Xenon atoms are placed in the channel in order to model their arrangement corresponding to the limiting stoichiometry of VA*0.5Xe.

Results and Discussion

The establishment of a consistent relationship between ^{129}Xe NMR parameters and properties of sorbent-xenon systems, both physical (macroscopic) and structural (molecular level), relies on detailed studies on a series of similar sorbents, where a property changes in small increments over a wide range.[22,30,31]

The micropores in the series studied have isolated 1D channels stretching parallel to the hexagonal axis of the crystal and having a well-pronounced chirality (Figure 2). The micropores display similar hydrophobic character and structural symmetry but vary in their geometry, with average diameter ranging from 3 to 5.4 Å and a helical displacement of the center from the central axis ranging from 0.1 to 1.1 Å for different dipeptides.[8]

Figure 3 illustrates CF HP ^{129}Xe NMR spectra of VA and AI dipeptides in the temperature range from 343 to 173 K showing signals corresponding to xenon in three different environments. The narrow signal at 0 ppm represents xenon atoms in the gas phase, the broader band that overlaps partially with the gas-phase signal and slightly shifted toward lower fields (centered at about 5 ppm at 343 K), can be ascribed to xenon adsorbed on the external crystal surfaces and in the intercrystallite regions. Finally, the most deshielded signal is from xenon absorbed in the nanochannels. At 343 K, the isotropic chemical shift of this signal is 126.7 ppm for VA and 137.6 ppm for AI. All materials demonstrate pronounced chemical shift anisotropy (CSA) with axial symmetry.

A decrease in temperature causes complex changes in the spectra, including the relative intensities, positions and line

(28) Moudrakovski, I. L.; Nossov, A.; Lang, S.; Breeze, S. R.; Ratcliffe, C. I.; Simard, B.; Santyr, G.; Ripmeester, J. A. *Chem. Mater.* **2000**, *12*, 1181–1183.
(29) Kunwar, A. C.; Turner, G. L.; Oldfield, E. *J. Magn. Reson.* **1986**, *69*, 124–127.
(30) Terskikh, V. V.; Mudrakovskii, I. L.; Mastikhin, V. M. *J. Chem. Soc., Faraday Trans.* **1993**, *89*, 4239–4243.
(31) Terskikh, V. V.; Moudrakovski, I. L.; Breeze, S. R.; Lang, S.; Ratcliffe, C. I.; Ripmeester, J. A.; Sayari, A. *Langmuir* **2002**, *18*, 5653–5656.

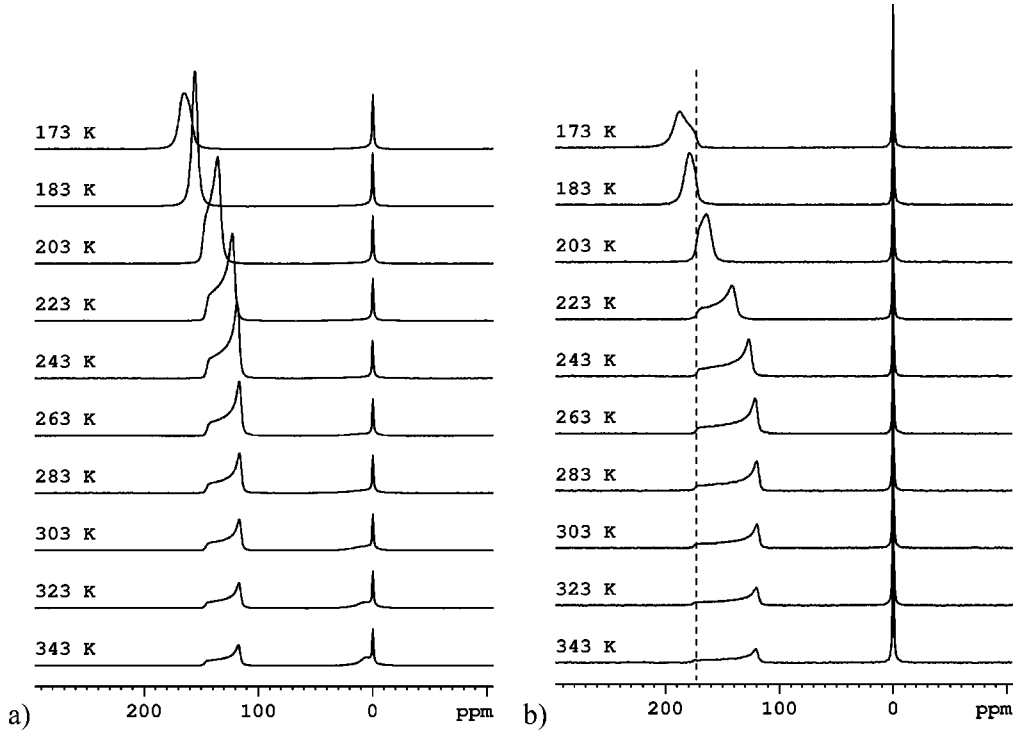

Figure 3. Experimental continuous-flow hyperpolarized ^{129}Xe NMR spectra for VA (a) and AI (b) dipeptides at variable temperature. The dashed line shows the constancy of the parallel component of the chemical shift tensor at variable temperatures in AI.

shapes. The signal from the intercrystalline xenon in VA experiences broadening and a slight shift toward lower fields, as well as a progressive decrease in intensity, leading to its complete disappearance below about 263 K. It should be noted that only the dipeptides AV and VA show this intercrystallite (or external surface) signal. In AV, it is observable even at 173 K and overlaps with the anisotropic signal in the temperature range of 243−263 K. AI also showed the intercrystallite adsorption of Xe, but only upon aging of the sample (see below).

At the reduced temperature, the signal from xenon absorbed in the nanochannels of VA and AI shows a significant downfield shift and an inversion of the anisotropy. The span of the CSA decreases with temperature, reaching a minimum around 183 K. At this temperature, a nearly isotropic signal is observed, the sign of the anisotropy being inverted at a lower temperature (173 K).

These general features are common to the spectra of all eight dipeptides studied in this work (a full set of spectra is given in the Supporting Information) and they are in qualitative agreement with other NMR studies on systems where xenon is absorbed in nanochannels.[8,13,32−40] At the same time, each dipeptide reveals its own characteristic spectra due to the sensitivity of the ^{129}Xe NMR parameters to the distinctive size and unique geometry of the nanochannels. In particular, the isotropic chemical shift ranges from 95.6 (AV) to 265.3 ppm (VI) at 343 K and from 149.0 (AV) to 280.6 ppm (VI) at 173 K.

Aging of Dipeptide Samples. The experiments conducted in this work were complicated by irreversible changes in the samples that resulted in an apparent decrease in microporosity. In particular, the decrease in intensity of the intrachannel xenon signal was observed down to its complete disappearance in some cases. Here the changes are referred to as aging to emphasize their irreversible nature and the fact that the changes progressed steadily in time. At least three different sources of aging were identified, as discussed below.

The first type of aging was inherent particularly in AV, VA, and AI. These three dipeptides, unlike the others, also showed intercrystallite adsorption, with the appearance of the intercrystallite signal (especially for AI) occurring after new samples were subjected to a sorption−desorption cycle. The presence or appearance of the intercrystallite signal was always associated with some loss in intensity of signal from xenon residing inside the nanochannels. In some cases, it was possible to visually observe disintegration of large single crystals (VA) that had been subjected to xenon pressure. ^{13}C

(32) Meersmann, T.; Logan, J. W.; Simonutti, R.; Caldarelli, S.; Comotti, A.; Sozzani, P.; Kaiser, L. G.; Pines, A. *J. Phys. Chem. A* **2000**, *104* (50), 11665–11670.
(33) Ueda, T.; Eguchi, T.; Nakamura, N.; Wasylishen, R. E. *J. Phys. Chem. B* **2003**, *107*, 180–185.
(34) Sozzani, P.; Comotti, A.; Simonutti, R.; Meersmann, T.; Logan, J. W.; Pines, A. *Angew. Chem., Int. Ed.* **2000**, *39* (15), 2695–2699.
(35) Sears, D. N.; Wasylishen, R. E.; Ueda, T. *J. Phys. Chem. B* **2006**, *110*, 11120–11127.
(36) Koskela, T.; Ylihautala, M.; Jokisaari, J. *Microporous Mesoporous Mater.* **2001**, *46*, 99–110.
(37) Ripmeester, J. A.; Ratcliffe, C. I. *J. Phys. Chem.* **1995**, *99*, 619–622.
(38) Springuel-Huet, M. A.; Fraissard, J. *Chem. Phys. Lett.* **1989**, *154* (4), 299–302.
(39) Ueda, T.; Kurokawa, K.; Eguchi, T.; Kachi-Terajima, C.; Takamizawa, S. *J. Phys. Chem. C* **2007**, *111*, 1524–1534.
(40) Comotti, A.; Bracco, S.; Ferretti, L.; Mauri, M.; Sozzani, P. *Chem. Comm.* **2007**, 350–352.
(41) Sholl, D. S.; Lee, C. K. *J. Chem. Phys.* **2000**, *112*, 817–824.
(42) Sircar, S.; Rao, M. B. Heat of Adsorption of Pure Gas and Multicomponent Gas Mixtures on Microporous Adsorbents. *Surfaces of Nanoparticles in Porous Materials*; Schwartz, J. A., Contescu, C., Eds.; Marcel Dekker: New York. 1999, Chapter 19, pp 501−528.
(43) Cao, D. V.; Sircar, S. *Adsorption* **2001**, *7*, 73–80.
(44) Myers, A. L. *AIChE J.* **2002**, *48*, 145–160.

of dipeptides with absorbed Xe show some pronounceable chemical shifts of the CH_3 groups exposed inside the channels (see the Supporting Information, Figure S3 and Table S1). These shifts reach almost 2 ppm for the dipeptides with the narrowest channels, but even for "moderately sized" pores of VA they exceed 1 ppm. Such prominent shifts caused by physical interaction with inert atom indicate some significant structural changes. Although the absorption and changes in the ^{13}C spectra appear to be completely reversible, the mechanical stress in different parts of the crystals may cause extensive cracking and breakage of the crystals. This explains the growth of the intercrystallite Xe signal, to some extent at the expense of the signal from the intrachannel xenon as relatively large crystals are transformed into fine crystals or a partially amorphous phase with a highly developed external surface. Such mechanical changes may occur every time as a sample passes through a certain loading point and in this way the sample "memorizes" how many sorption−desorption cycles it has experienced.

The second type of aging was observed particularly for VA but might, at some point, become a nuisance for any of the dipeptides under study. As reported earlier,[8,14] VA in its microporous hexagonal form has a packing coefficient of 0.537(4), which is too low for a stable molecular crystal, even taking into account stabilization by hydrogen bonds. Therefore, the existence of a more stable, dense polymorphic form of VA could not be excluded (note that it is impossible to prove the nonexistence of such polymorph). The problem with the dense form is of kinetic origin: the microporous form exists as a metastable polymorph for kinetic reasons but starts to disappear upon contact with the seeds of a stable dense polymorph once they appear in the surroundings. Extensive experiments with VA samples eventually generated the stable form of the dipeptide and an almost complete disappearance of microporosity was observed in some samples after less than two months of work. The polymorphic transition appears to be irreversible and occurs for kinetic reasons; a guest component (xenon in our case) does not necessarily participate but, as in other previously described systems,[45,46] may act, especially in combination with temperature changes, as a catalyst. The study of the new polymorph is currently underway.

The third type of aging is likely an intrinsic property of all the dipeptides studied. The organization of micropore space in narrow, mutually isolated (noninterconnected) nanochannels makes such systems subject to easy "poisoning" by the presence of defects in their crystal structure or low-volatility impurities. The defects may appear as stacking faults between crystallite domains[47] or as molecular-size irregularities. Hypothetically, it could be due to a partial oxidation of the external surface during materials exposure to the air. Such oxidation may lead to the formation of the surface carboxylic groups, which could block the entrance to the channels either by themselves or by forming hydrogen bonds with adsorbed water. The impurities may completely block the nanochannels even in relatively low concentrations. Noteworthy, "poisoning" of zeolite catalysts due to blockage of micropores is one of the major problems in industry; chabazite,[48] mordenite,[48,49] faujasite,[50] and ferrierite[51] were reported as being subject to this phenomenon. In peptide-based microporous materials, the problem is rather worse: the impurities cannot be removed by thermal or chemical treatment because of the limited stability of these materials, and the dipeptides can even produce such impurities themselves as a result of their steady degradation.

We should note that the adsorption of water alone can not account for the observed changes in sorption properties of dipeptides. If water content provided an important contribution to sample aging, its effect would be the most pronounceable in hydrophilic dipeptides, while our observations on LS dipeptides are not significantly different from others materials. Moreover, aging is not only observed as a function of time, but it is increased when samples are subjected to several sorption−desorption cycles with exposure to air between the cycles. The gas stream in experiments can be considered completely free of water after passing through several high efficiency traps, and we can rule out that water alone has a significant role in the aging processes. At this point one may only speculate that the observed aging of the samples is a combination of several processes.

Thermodynamics of Sorption from Signal Intensities and Isotropic Chemical Shifts. *Thermodynamic Parameters from Signal Intensities: High-Temperature Region, Low Loadings.* As a typical example, the temperature dependence of the integrated CF HP ^{129}Xe NMR signal intensities ($I = I_{ch}/I_{gas}$) obtained for VV is shown in Figure 4a. An exponential increase of I upon cooling from approximately 340 to 220 K is followed by a decline at lower temperatures (from 200 to 170 K), with a maximum being observed at some intermediate temperature range between 220 and 200 K.

This dependence is a result of two opposite effects. On the one hand, the low temperature results in higher channel loading. On the other hand, reduced temperature has a negative kinetic effect, slowing the diffusion of xenon inside the nanochannels. The condition of fast diffusion is a critical factor in hyperpolarized ^{129}Xe NMR as it provides a continuous replacement of the xenon nuclei that relax to a thermally polarized state (and therefore become nearly undetectable) with new hyperpolarized xenon. In the high-temperature region, the intensity of the NMR signal is merely controlled by the thermodynamics of xenon adsorption in the dipeptide channel and the ratio $I_{channel}/I_{gas}$ is indeed representative of the relative amount of xenon absorbed. In the low-temperature region, the kinetic factors become dominant: reduced diffusion, which is defined by the temperature-dependent diffusion constant D_0, slows the

(45) Soldatov, D. V.; Ripmeester, J. A.; Shergina, S. I.; Sokolov, I. E.; Zanina, A. S.; Gromilov, S. A.; Dyadin, Y. A. *J. Am. Chem. Soc.* **1999**, *121*, 4179–4188.
(46) Soldatov, D. V.; Ripmeester, J. A. *Chem.−Eur. J.* **2001**, *7*, 2979–2994.
(47) Newsam, J. M.; Deem, M. W. *J. Phys. Chem.* **1995**, *99*, 8379–8381.
(48) Barrer, R. M.; Rees, L. V. *Trans. Faraday Soc.* **1954**, *50*, 989–999.
(49) Mori, N.; Nishiyama, S.; Tsuruya, S.; Masai, M. *Appl. Catal.* **1991**, *74*, 37–52.
(50) Flego, C.; Kiricsi, I., Jr.; Clerici, M. G. *Appl. Catal., A* **1995**, *124*, 107–119.
(51) Van Donk, S.; Bus, E.; Broersma, A.; Bitter, J. H.; de Jong, K. P. *Appl. Catal., A* **2002**, *237*, 149–159.

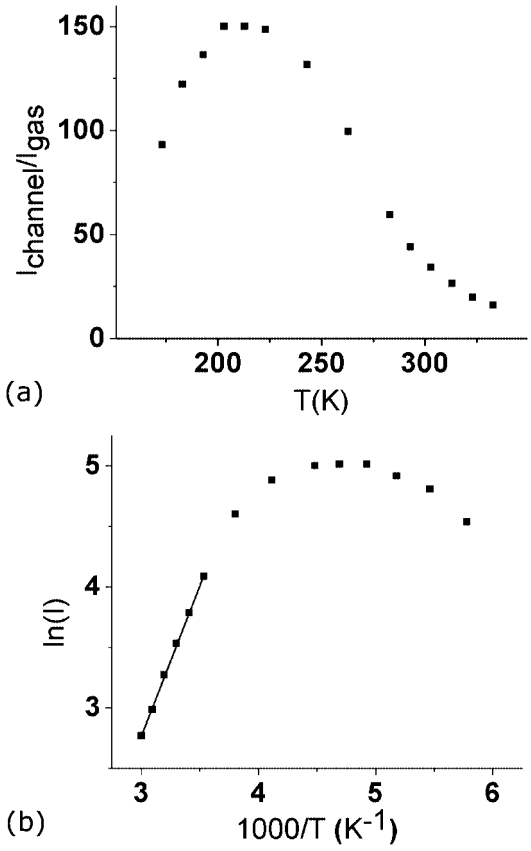

Figure 4. (a) Signal intensities $I = I_{ch}/I_{gas}$ for VV dipeptide as a function of temperature. (b) The same data presented in the ln(I) versus 1000/T coordinates and fitting of the data with a straight line (high-temperature region).

process of the replacement of relaxed xenon with hyperpolarized nuclei, causing a significant loss of signal. Similar behavior has been observed for sorption of xenon in tris(*o*-phenylenedioxy)cyclotriphosphazene (TPP) nanochannels[32] and this might be expected for other sorbents having their micropore space organized in isolated narrow channels. To extract quantitative information on the sorption process from the intensities of the HP ^{129}Xe NMR signal, therefore, only the high-temperature region, where the diffusion of xenon in the nanochannels is fast, should be considered.

Assuming that xenon can fill a limited number of discrete sorption sites in the nanochannels, the sorption process can be described by the following equation:

$$[\ ]_{solid} + Xe_{gas} = [Xe]_{solid} \quad (1)$$

where [ ] represents a single sorption site and [Xe] denotes an occupied sorption site. The equilibrium (sorption) constant for the process (K) is the ratio of activities for adsorbed Xe and xenon in the gas phase. This ratio is proportional to experimentally measured ratio of the signal intensities

$$K = k_{probe}(I_{channel}/I_{gas}) = k_{probe}I \quad (2)$$

where k_{probe} is a coefficient defining the volumes ratio for the gas and sorbent in the coil region of the probe. The coefficient depends on how the sample was packed in the probe and its precise value is unknown (the estimated value for highly packed fine powders $k_{probe} \approx 1$). Sets of experiments conducted on the same sample show that k_{probe} remains almost constant as long as the same probe in the same instrumental configuration is used.

The sorption constant K, on the other hand, is directly related to the standard free energy of the process (1) ($\Delta G°$) and can be expressed as follows

$$K = e^{-\Delta G°/RT} = e^{\Delta S°/R}e^{q_{st}/RT} = k_0 e^{q_{st}/RT} \quad (3)$$

where $\Delta S°$ is the standard entropy change in process 1, k_0 is a "pre-exponential coefficient" (entropy term that does not depend on temperature), and q_{st} is the isosteric heat of sorption,[41,42] which refers to a particular loading and equals, with opposite sign, the isosteric sorption enthalpy of process 1. Combination of eqs 2 and 3 gives the expression for integral intensity of the intrachannel xenon as function of temperature

$$I(T) = \frac{k_0}{k_{probe}} \cdot e^{q_{st}\ /\ RT} = ke^{q_{st}\ /\ RT} \quad (4)$$

where $k = k_0/k_{probe}$ is a temperature-independent term. In coordinates ln (I) versus 1/T, the experimental data may be fitted with a straight line according to the linear equation

$$\ln(I) = \ln(k) + \frac{q_{st}}{R}\frac{1}{T} \quad (5)$$

with the intercept ln(k) and slope q_{st}/R.

Plots of ln(I) versus 1/T (Figure 4b and the Supporting Information, Figure S2) do show a linear segment in the high-temperature region, where sorption equilibrium is established. In the low-temperature region, significant deviations from linearity are observed indicating that even though thermodynamic equilibrium was established, the method used is not suitable because only a small percentage of the adsorbed xenon atoms can be detected. The fitting of experimental points in the high-temperature region provides values for isosteric heats of sorption and k (as an estimate of k_0) in the observed temperature intervals, the values being valid for low loadings (Table 1). The correlation factors for the fitted regions are higher than 0.99, indicating an excellent agreement of the experimental data with the model applied.

Isotropic Chemical Shifts vs Temperature. The analysis of isotropic chemical shifts (δ_{iso}) provides another, independent method of monitoring sorption changes with temperature. In contrast to signal intensities, which are defined by the total amount of the intrachannel HP ^{129}Xe atoms, chemical shifts are influenced by Xe−Xe interactions and contain information on the density of the HP ^{129}Xe atoms inside the nanochannels. The temperature dependence of the isotropic chemical shift for xenon atoms inside the channels is expected to consist of three regions (Figure 5). In high-temperature region A, the concentration of xenon atoms in the nanochannels is very low; the chemical shift δ_s is defined by Xe−wall interactions only and corresponds to the shielding of a single xenon atom in the empty channel. In lowest-temperature region C, the concentration of xenon in the nanochannels reaches its saturation. The chemical shift δ_f is defined by both Xe−wall and Xe−Xe interactions and corresponds to 1D close packing of xenon atoms inside the channel, with Xe−Xe interactions dominating the observed shielding. The low-temperature region B represents an intermediate situation, where the concentration of xenon

Table 1. Thermodynamic Parameters of Xenon Sorption in the Studied Dipeptides Derived from the Experimental Data for the Indicated Temperature Intervals (K): Isosteric Heats of Sorption q_{st} (kJ/(mol of Xe)), k, and k'

	analysis of signal intensities (high temperatures, low loadings)			analysis of chemical shifts (low temperatures, high loadings)		
sample	T-range[a]	$k \times 10^3$	q_{st}	T-range[a]	$k' \times 10^3$	q_{st}
AV	343−293 (5)	30.8 ± 0.9	8.21 ± 0.08	273−173 (11)	4.8 ± 1.4	20.80 ± 0.54
	293−273 (3)	1.1 ± 0.2	16.51 ± 0.59			-
VA	333−293 (4)	22.4 ± 1.8	12.16 ± 0.23	253−173 (9)	2.4 ± 0.7	20.96 ± 0.50
	293−253 (5)	8.4 ± 1.0	14.42 ± 0.28			-
LS	333−293 (5)	5.9 ± 1.4	20.07 ± 0.72	253−173 (9)	6.5 ± 2.5	20.54 ± 0.71
AI	343−323 (3)	1.1 ± 0.4	19.00 ± 1.11	273−183 (10)	8.0 ± 4.3	20.84 ± 1.02
	323−283 (5)	7.4 ± 1.0	14.01 ± 0.37			-
VV	333−283 (6)	9.1 ± 1.2	20.69 ± 0.36	293−173 (10)	8.9 ± 2.8	19.81 ± 0.57
IA	333−293 (3)	1.8 ± 0.4	17.67 ± 0.65	273−173 (6)	5.5 ± 0.5	17.8[b]
IV	343−253 (5)	4.8 ± 1.0	17.76 ± 0.56	213−173 (5)	7.5 ± 1.3	17.8[b]
VI	293−193 (6)	2.6 ± 0.4	17.01 ± 0.37			

[a] The number of experimental points used in the fit is given in brackets. [b] Fixed value.

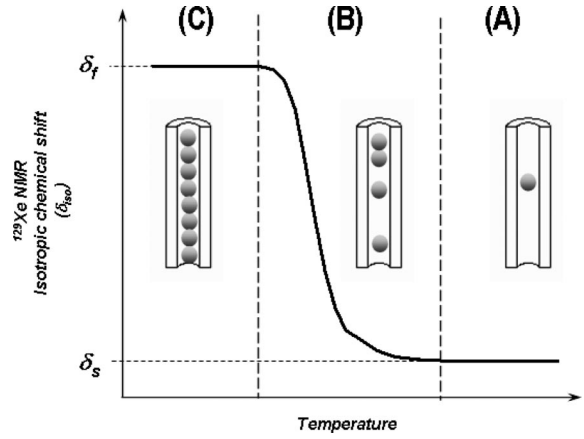

Figure 5. Schematic representation of the ideal change of isotropic chemical shift for intrachannel Xe with temperature at isobaric conditions (assuming that Xe−wall interactions are not temperature dependent, xenon atoms freely enter 1D cylindrical pores, and the pore structure remains rigid upon guest inclusion). The drawings show the cross-section of ideal nanochannels at different loadings corresponding to different temperature regions.

atoms in the nanochannel and average chemical shift of the atoms smoothly grow from their minimal to their maximal values.

Experimentally observed variations of the chemical shift with temperature are summarized in Figure 6. The experimental dependencies have sigmoid character and follow, in general, the expected trend as shown in Figure 5. Regions A and B are demarcated at ∼250 K for most dipeptides; plateau C is not reached in any of the systems but the presence of inflection points around 180 K (except for dipeptides having the narrowest channels, IA, VI, and IV) indicate that it would be at lower temperatures.

In high-temperature region A, the experimental ^{129}Xe isotropic chemical shifts follow different trends for different dipeptides. Four of them (AV, VA, AI, and LS) show a decrease, a minimum being reached between 260 and 280 K. The chemical shift in region A for VV and IA is almost constant. The last two (IV and VI) show a linear increase in δ_{iso}. As already mentioned, Xe−Xe interactions in this region are negligible and the observed shielding is mainly affected by interaction with the atoms of the channel walls (Xe−wall). There is a clear dependence of the observed trends on the diameter of the channels that vary in the sequence AV > VA > LS > AI > VV > IA > IV > VI (experimental data from He pycnometry[8]). A more detailed theoretical study

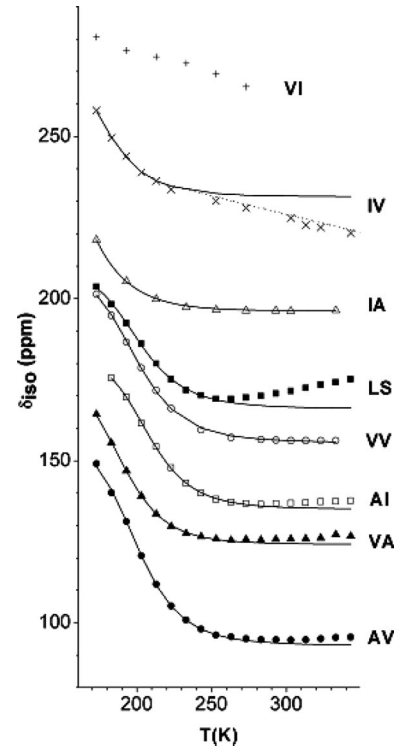

Figure 6. Variation of the experimental ^{129}Xe NMR isotropic chemical shift (δ_{iso}) as a function of temperature for the eight dipeptides AV (closed circles), VA(closed triangles), AI(open squares), VV(open circles), LS (closed squares), IA (open triangles), IV(side-crosses), and VI (plus-signes). Solid lines represent the fitting of the experimental points according to the thermodynamic model discussed in the text. The dotted line is the fit to a straight line relative to the linear behavior of δ_{iso} observed in IV in the high-temperature region.

(e.g., one-body distribution functions of Xe in all of the dipeptide channels) would be required in order to obtain complete information on the temperature dependence of Xe−wall interactions in different dipeptides. Nevertheless, the guidelines provided by the previous theoretical works[13,52–57] and our experimental results suggest the following possible explanation for the observed temperature dependence of the isotropic chemical shifts on the diameter of the channel.

In this temperature region, the isotropic chemical shift depends not only on the average diameter of the nanochannel but also on the time-averaged distribution of xenon species between the widest parts of the nanochannel and its more constricted parts such as narrower passages and side niches.

It was demonstrated previously[58] that the ability of guest species to enter side niches/pockets can dramatically alter the process of sorption. As the temperature increases, the constricted parts become more populated resulting in increased average shielding and higher values of the isotropic chemical shift (this can be better understood by considering the chemical shift anisotropy of the observed signals and will be analyzed in more detail later). This effect might be expected when included xenon species have some translational degrees of freedom, especially perpendicular to the channel axis direction, that is, for nanochannels with diameters greater than the van der Waals diameter of Xe (~4.3 Å). Indeed, an increase of the chemical shift with temperature is observed for AV, VA, AI and LS dipeptides having their average channel diameters in the range 4.3−5.4 Å. In dipeptides with narrower channels, VV (4.0 Å) and IA (3.6 Å), the dynamics of the xenon atoms is much more restricted and the chemical shift is almost independent of temperature. Finally, in dipeptides with very narrow nanochannels, IV (3.4 Å) and VI (3.0 Å), the xenon species have very little translational freedom as the flexible matrix adjusts by a local widening suitable for accommodating xenon species. The behavior of the observed chemical shift for these dipeptides is consistent with the presence of sites having a proper diameter for the xenon to fit in registery.[37] In other words, absorbed xenon atoms appear to be tightly bound to the structure and their chemical shifts increase upon cooling because of thermal contraction of the entire crystal.

In low-temperature region B, the isotropic chemical shift increases steeply with decreasing temperature, showing a distinctive curvature for each dipeptide. In this region the xenon atoms approach each other and the contribution from Xe−Xe interactions to the isotropic chemical shift becomes comparable with the contribution from Xe−wall interactions. At the lower temperature more xenon atoms occupy the nanochannels and the average Xe−Xe distance shortens. A contribution from the Xe−Xe interactions will reach an upper limit once the nanochannels are completely filled with densely packed xenon atoms (region C in Figure 5). Neither of the two limiting cases, xenon in empty and completely filled channels, can be seen easily in the experimentally observed shifts. At higher temperatures the chemical shifts are affected strongly by the temperature dependence of Xe−wall interactions, whereas at lower temperatures, possible condensation of xenon below 170 K could hinder the continuous flow measurements and monitoring of the highest loadings.

The filling of the narrowest channels (IA, VI, and IV) appears to be different from the ideal situation as illustrated in Figure 5. Neither of the dipeptides demonstrates an inflection point that would imply region C is approached in the temperature range studied. This observation indicates that the xenon atoms are so tightly trapped by the walls of these narrow channels that the average interatomic distance between xenon atoms remains much larger than that in the bigger nanochannels, even at the lowest temperatures. Similar behavior has been observed already for other materials with 1D channels.[35] The presence of the channel constrictions, however, is likely to result from the structural flexibility of the dipeptides rather than from fixed protrusions into the nanochannels. In fact, the observation of a change in the temperature dependence of the chemical shift from linear (region A) to sigmoid (region B) in IV and VI suggests that the effect of the channel structure on the sorption process varies with loading.

Thermodynamic Parameters from Chemical Shifts: Low-Temperature Region, High Loadings. In the low-temperature region, the exchange of xenon between solid dipeptide and the gas phase is slower and becomes comparable with the lifetime of HP ^{129}Xe. Therefore, the ratio of signal intensities $I = I_{ch}/I_{gas}$ is no longer representative of the actual distribution of xenon between the gas and sorbent phases as defined by the sorption equilibrium. However, the near-surface portion of bulk dipeptide is still quite accessible to the HP ^{129}Xe atoms. This portion is representative of the bulk because the micropore structure of the dipeptide is homogeneous in the crystals. Therefore, the chemical shifts can still be used to describe the quantitative thermodynamics of sorption in the low-temperature region.

Previously studied xenon sorption isotherms for AV and VA[14] appeared to follow the Langmuir equation

$$\Theta_{rel} = \frac{K_L p}{1 + K_L p} \tag{6}$$

where Θ_{rel} is the relative coverage (a fraction of the total sorption sites occupied by xenon atoms, $0 < \Theta_{rel} < 1$), K_L is a Langmuir constant, and p is the xenon pressure at equilibrium. To show the dependence of the relative coverage on temperature, eq 6 should be written in a more general form[28,59,60]

$$\Theta_{rel}(T,p) = \frac{pk' e^{q_{st}/RT}}{\sqrt{T} + pk' e^{q_{st}/RT}} \tag{7}$$

where k' is the temperature-independent portion of the Langmuir constant and q_{st} is the isosteric heat of sorption already mentioned previously. It should be noted that the square root of temperature is always a part of the Langmuir[59] constant in (eq 6) but it is not evident as long as the equation is applied to sorption isotherms (T = const). Equation 7 is quite general, as it may be applied to both sorption isotherms and sorption isobars. In the experiments of this work, the partial pressure of xenon is maintained constant (0.01 bar), whereas temperature is varied. Therefore, the coverage in the experiment changes isobarically.

(52) Jameson, C. J.; de Dios, A. C. *J. Chem. Phys.* **1992**, *97* (1), 417–434.
(53) De Dios, A. C.; Jameson, C. J. *J. Chem. Phys.* **1997**, *107* (11), 4253–4270.
(54) Jameson, C. J.; de Dios, A. C. *J. Chem. Phys.* **2002**, *116* (9), 3805–3821.
(55) Jameson, C. J. *J. Am. Chem. Soc.* **2004**, *126*, 10450–10456.
(56) Sears, D. N.; Vukovic, L.; Jameson, C. J. *J. Chem. Phys.* **2006**, *125*, 114708–114722.
(57) Jameson, C. J. *J. Chem. Phys.* **2002**, *116* (20), 8912–8929.
(58) Nagano, J.; Eguchi, T.; Asanuma, T.; Masui, H.; Nakayama, H.; Nakamura, N.; Derouane, E. G. *Microporous Mesoporous Mater.* **1999**, *33*, 249–256.
(59) Langmuir, I. *J. Am. Chem. Soc.* **1918**, *40*, 1361–1403.
(60) Ranke, W.; Joseph, Y. *Phys. Chem. Chem. Phys.* **2002**, *4*, 2483–2498.

To relate the observed chemical shift to the relative coverage, we recall the equation proposed by Fraissard and co-workers[22]

$$\delta_{obs} = \delta_0 + \delta_s + \delta_{Xe-Xe} + \delta_M \quad (8)$$

where δ_0 is the reference (gaseous xenon at zero pressure), δ_s arises from interactions with the inner surface of the pores (Xe−wall), δ_{Xe-Xe} corresponds to interatomic interactions between absorbed xenon atoms, and δ_M accounts for magnetic fields from paramagnetic ions if they are present in the porous material. The last term δ_M is zero in our case and δ_0 is zero by convention. As discussed in the previous section, Xe−wall interactions expressed by δ_{obs} define the observed chemical shift in the high-temperature region. In this region, the Xe−wall interactions depend on temperature due to the dynamics of the absorbed species over the cross-section of the nanochannel. Therefore, the variation of δ_{obs} in this region is dependent on temperature and is likely to be independent of loading. In the low-temperature region, Xe−Xe interactions start to dominate and the only coverage-dependent term of eq 8, δ_{Xe-Xe}, becomes a significant contributor to the chemical shift. The chemical shift observed at any particular temperature can be considered as a sum of the chemical shift defined by the Xe-walls interactions in the empty nanochannels (δ_s) and a fraction of the total chemical shift variation $\Delta\delta = \delta_f - \delta_s$ (Figure 5) between the chemical shifts corresponding to the completely filled (δ_f) and empty (δ_s) nanochannels

$$\delta_{obs} = \delta_s + \Delta\delta\Theta_{rel} \quad (9)$$

Previously, such an approach proved to be valid in fitting experimentally determined xenon sorption isotherms for zeolites.[61]

Combining eqs 7 and 9, we obtain the dependence of the observed chemical shift on pressure and temperature

$$\delta_{obs} = \delta_s + \Delta\delta\frac{pk' e^{q_{st}/RT}}{\sqrt{T} + pk' e^{q_{st}/RT}} \quad (10)$$

Under the experimental conditions of this work, $p = 0.01$ (relative pressure, dimensionless) and the dependence $\delta_{obs}(T)$ becomes an isobar, a sigmoid-shaped curve defined by four parameters: δ_s, $\Delta\delta$, k', and q_{st}. To simplify the task of fitting the experimental data with eq 10, δ_s was found from the extrapolation of the chemical shifts in the high-temperature region. The value of δ_s was assumed to be constant in the lower-temperature region considered (region B in Figure 5), as it is relatively narrow and the dynamics of xenon species responsible for the deviation of the observed chemical shifts from δ_s is expected to be suppressed at higher loadings. Fitting of experimental data with (eq 10) is shown in Figure 6 (solid lines) and the derived values of k', q_{st}, δ_s,and $\Delta\delta = \delta_f - \delta_s$ are reported in Tables 1 and 2. It should be mentioned that fitting was impossible for the narrowest channel of VI. For IA and IV, it was necessary to fix q_{st} to the values obtained from the signal intensities in high-temperature region.

Thermodynamics of Sorption: Discussion. The thermodynamic description of sorption is a primary fundamental account of a sorbent material that defines its applicability to a desired separation, purification, storing, or catalytic process. On the other hand, the investigation of the relation between the thermodynamic parameters of sorption and structural parameters of the sorbent−sorbate components reveals issues defining the energetics and selectivity of sorption and contribute to the design of new porous materials. The development of numerous synthetic zeolites and their industrial applications were accompanied by extensive and detailed sorption studies documented in the literature.[62]

Table 2. Isotropic Chemical Shifts (ppm) of Absorbed ^{129}Xe at Zero Loading (δ_s) and Their Total Variations ($\Delta\delta$) Calculated from the Experimental Data for Dipeptides Studied

	calcd chemical shift variation with temperature	
sample	δ_s	$\Delta\delta = \delta_f - \delta_s$
AV	93.0	63.6
VA	124.1	50.3
LS	166.0	42.0
AI	134.6	53.8
VV	155.0	53.2
IA	196.3	43.8
IV	231.4	46.0
VI	-	-

The thermodynamic parameters of sorption experimentally derived in this study are summarized in Table 1. In general, the sorption of xenon in all eight dipeptides is energetically very favorable, as judged from the q_{st} values of 8−21 kJ/(mol of Xe). Characteristically, at high loadings, the heats of sorption are similar, whereas at low loadings, they vary; the variation are obviously related to the variation in the sorption entropy. This result likely indicates that at high loadings and low temperatures in all the channels, there is similar dense packing of xenon atoms having like environments and low degrees of freedom. This similarity is observed in spite of substantially different sizes of the channels and may signify the change in channel structure induced by the absorbed xenon atoms.

In contrast, at low loadings and high temperatures, different situations may arise, with various degrees of freedom of the xenon species in the channel. This possibility is especially well illustrated by stepwise changes in AV, VA, and AI dipeptides, implying possible phase transitions in these dipeptides. From the comparison of thermodynamic parameters in the two temperature intervals (Table 1), the enthalpies and approximate temperatures of the phase transitions are 8.3(6), 2.3(4), and −5(1) kJ/(mol of Xe) and 298, 298, and 323 K for AV, VA, and AI, respectively. The entropy terms change in order to compensate for the contribution of the enthalpy changes to the free energy. This phenomenon is known as a compensation effect and has been observed previously in zeolites.[63] A higher ordering of the absorbed species in the channel ensures a better interaction with the environment (favorable enthalpy term) but it also implies some loss of freedom (unfavorable entropy term), whereas a higher mobility creates the opposite effects.

The phase transitions in the dipeptide−xenon inclusion compounds are likely to arise from a not very dramatic but

(61) Kato, N.; Ueda, T.; Hironori, O.; Miyakubo, K.; Eguchi, T. *Phys. Chem. Chem. Phys.* **2004**, *6*, 5427–5434.

(62) Breck, D. W. *Zeolite Molecular Sieves. Structure, Chemistry, and Use*; Wiley, New York, 1974.

(63) Takaishi, T.; Yusa, A.; Amakasu, F. *J. Chem. Soc., Faraday Trans.* **1971**, *67*, 3565–3576.

stepwise structural adjustment in the dipeptide matrix, or packing of xenon atoms inside the nanochannels. As can be seen from the enthalpy and entropy changes, there are less efficient interactions but more degrees of freedom in the higher-temperature modifications of AV and VA. Therefore, cooling might induce a better fit between a xenon atom and a sorption site and higher degree of guest ordering in the nanochannels. Phase transitions of this kind have been observed and studied in other inclusion compounds and may be induced by either temperature[64–69] or guest loading.[70,71] In a case of AI, the increase in entropy and decrease in q_{st} might be a result of a stepwise increase in the channel diameter that takes place at a certain level of loading. Such phase transitions are triggered at a certain "gate pressure" of the guest.[72–76] Possible structural motifs in the lower-temperature phases may be seen in recent studies showing that the hexagonal structure of AV transforms into a superstructure with four symmetrically nonequivalent channels upon inclusion of 2-propanol/water (120 K)[77] and the hexagonal structure of VA distorts to monoclinic in its inclusion compound with acetonitrile/water (105 K).[78] In general, the observed phase changes in the dipeptides studied characterize them as stimuli-responsive host materials.[5,79]

With the reduced channel the heats of sorption (Table 1) either increase or within experimental error remain almost unchanged (low temperatures and high loadings). Although the temperature dependence of isosteric heats of sorption is generally considered to be weak and may be neglected, the increase of q_{st} with loading is usually ascribed to the presence of strong lateral interactions between molecules of sorbate within the micropores. In general, the isosteric heat of sorption is affected by a number of factors and previous studies on sorption in zeolites suggest that it may be a complex function of loading.[80–85] Other studies indicate that deformation of the sorbent may contribute significantly to the variation of q_{st},[86,87] the factor being important for the flexible sorbent as materials of this study.

The thermodynamic values derived in this work may be compared with those of zeolites and some other porous materials. Zeolites present host frameworks with much stronger local charges distributed over the crystal framework that may imply stronger inductive host−guest interactions. Another major distinction is the rigidity of the zeolite framework. At the same time, zeolites may reveal similarity to the materials of this work in the topology of their micropores. Sorption of xenon in 1D channels of ferrierite having 4.2×5.4 Å^2 cross-section dimensions[88] is characterized by an initial (lowest loading) q_{st} of 31.4 kJ/mol.[89,90] Sorption of xenon in the 1D channels of mordenite[88] (6.5×7.0 Å^2) is characterized by an initial q_{st} of 35.1 kJ/mol.[91] Sorption of xenon in the 3D system of channels in Linde 5A zeolite (diameter ~5 Å)[88] is accompanied by an initial q_{st} of 22.5 kJ/mol, which increases to ~25 kJ/mol at higher loading. Sorption of xenon in 3D system of channels in silicalite[88] (structural type ZSM-5, 5.3×5.6 Å^2 and 5.1×5.5 Å) is accompanied by an initial q_{st} of 26.6 kJ/mol.[92] From another study,[93] the sorption of argon, methane and sulfur hexafluoride in silicalite is characterized with k_0 of 50×10^{-3}, 27×10^{-3}, and 3.7×10^{-3}, respectively. The sorption of xenon in the 3D system of channels in faujasite[88] (NaX, diameter ~7.4 Å) is accompanied by an initial q_{st} of 19.2 kJ/mol and k_0 of 7.4×10^{-3} (zero filling, 193 K).[94] In one study, sorption of xenon in an organo-clay with ~6 Å micropores was reported with a q_{st} of 14 kJ/mol.[24] As one can see, the thermodynamic characteristics of the materials in the present study with respect to the sorption of xenon are very similar to those in zeolites, even with all the differences mentioned above. This may well imply that the sorption process is mainly controlled by van der Waals forces and is defined to the greatest extent by the fit between the xenon atom and the host cavity. Similar conclusions for silicalite were made from molecular dynamics simulations.[95] It can also be speculated that the advantage of zeolites as sorbents ascribed to the presence of local charges may be partially compensated by flexibility of dipeptide matrices that can provide better xenon-cavity fits by adjusting the pore structure during the course of sorption.

It is interesting to follow the changes in the isosteric heat of sorption with the diameter of nanochannels in the series

(64) Soldatov, D. V.; Kolesov, B. A.; Lipkowski, J.; Dyadin, Y. A. *J. Struct. Chem.* **1997**, *38*, 819–828.
(65) Mayo, S. C.; Welberry, T. R.; Bown, M.; Tarr, A. *J. Solid State Chem.* **1998**, *141*, 437–451.
(66) Soldatov, D. V.; Enright, G. D.; Ripmeester, J. A.; Lipkowski, J.; Ukraintseva, E. A. *J. Supramol. Chem.* **2001**, *1*, 245–251.
(67) Yeo, L.; Harris, K. D. M.; Kariuki, B. M. *J. Solid State Chem.* **2001**, *156*, 16–25.
(68) Nishikiori, S.; Takahashi, A.; Ratcliffe, C. I.; Ripmeester, J. A. *J. Supramol. Chem.* **2002**, *2*, 483–496.
(69) Majda, D.; Makowski, W. *Stud. Surf. Sci. Catal.* **2005**, *158*, 1161–1168.
(70) Takaishi, T.; Tsutsumi, K.; Chubachi, K.; Matsumoto, A. *J. Chem. Soc., Faraday Trans.* **1998**, *94*, 601–608.
(71) Huang, Y.; Leech, J. H.; Havenga, E. A.; Poissant, R. R. *Microporous Mesoporous Mater.* **2000**, *48*, 95–102, and refs 1−4 therein.
(72) Seki, K. *Phys. Chem. Chem. Phys.* **2002**, *4*, 1968–1971.
(73) Takamizawa, S.; Nakata, E.; Saito, T.; Yokoyama, H. *Inorg. Chem. Commun.* **2003**, *6*, 1326–1328.
(74) Takamizawa, S.; Saito, T.; Akatsuka, T.; Nakata, E. *Inorg. Chem.* **2005**, *44*, 1421–1424, and ref 12f therein.
(75) Uemura, K.; Kitagawa, S.; Fukui, K.; Saito, K. *J. Am. Chem. Soc.* **2004**, *126*, 3817–3828.
(76) Halder, G. J.; Kepert, C. J. *Aust. J. Chem.* **2006**, *59*, 597–604.
(77) Görbitz, C. H. *Acta Crystallogr., Sect. B* **2002**, *58*, 849–854.
(78) Görbitz, C. H. *CrystEngComm* **2005**, *7*, 670–673.
(79) Soldatov, D. V. *J. Inclusion Phenom.* **2004**, *48*, 3–9.
(80) Barrer, R. M.; Davies, J. A. *Proc. R. Soc. London, Ser. A* **1971**, *322*, 1–19.
(81) Thamm, H. *Zeolites* **1987**, *7*, 341–346.
(82) Shen, D.; Bülow, M. *Microporous Mesoporous Mater.* **1998**, *22*, 237–249.
(83) Pulin, A. L.; Fomkin, A. A. *Russ. Chem. Bull.* **2004**, *53*, 1630–1634.
(84) Fomkin, A.A. *Adsorption* **2005**, *11*, 425–436.
(85) Chakraborty, A.; Saha, B. B.; Koyama, S.; Mg, K. C. *Appl. Phys. Lett.* **2006**, *89*, 171901–171903.
(86) Jakubov, T. S.; Mainwaring, D. E. *Phys. Chem. Chem. Phys.* **2002**, *4*, 5678–5682.
(87) Ustinov, E. A.; Do, D. D. *Carbon* **2006**, *44*, 2652–2663.
(88) Meier, W. M.; Olson, D. H. *Atlas of Zeolite Structure Types*; Butterworth-Heinemann, London, 1992.
(89) Takaishi, T. *Pure Appl. Chem.* **1986**, *58*, 1375–1382.
(90) Takaishi, T.; Nonaka, K.; Okada, T. *J. Chem. Soc., Faraday Trans.1* **1987**, *83*, 3317–3329.
(91) Barrer, R. M.; Peterson, D. L. *Proc. R. Soc. London, Ser. A* **1964**, *280*, 466–485.
(92) Bülow, M.; Härtel, U.; Müller, U.; Unger, K. K. *Ber. Buns. Phys. Chem.* **1990**, *94*, 74–76.
(93) Myers, A. L. *Colloids Surf., A* **2004**, *241*, 9–14.
(94) Kiselev, A. V.; Du, P. Q. *J. Chem. Soc., Faraday Trans. 2* **1981**, *77*, 1–15.
(95) Ermoshin, V. A. *Russ. J. Phys. Chem.* **2002**, *76*, 1127–1131.

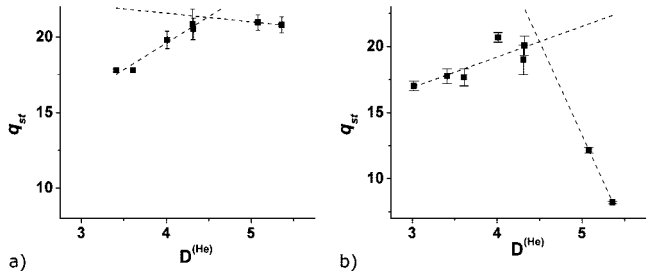

Figure 7. Heats of sorption q_{st} (kJ/(mol of Xe)) plotted as a function of the pore diameter (Å) (experimental data from helium pycnometry[8]). The values for q_{st} correspond to (a) high loadings, low temperatures (from isotropic chemical shifts) and (b) low loadings, high temperatures (from signal intensities). Dashed lines are linear fittings to guide the eye.

studied. As the driving force for the absorption is the affinity between the guest and the pore walls, pores with dimensions complementary to the diameter of xenon might be expected to result in a higher heat of sorption due to the optimal guest−host contacts.[26] Figure 7 shows q_{st} versus channel diameter (from He pycnometry[8]) for the series studied. As becomes apparent from the Figure, the highest heat of sorption occurs for a channel with a diameter of ∼4.4 Å, which is virtually equal to the diameter of the xenon atom. It is also interesting that the decrease of the channel diameter to values lower than 4.4 Å causes only a slight decrease in the sorption energy. Again, this result must be a consequence of the high flexibility of the dipeptide matrices where the close contact of the channel with Xe requires some expansion.

Characterization of Sorption at the Microlevel. *Chemical Shift Anisotropy.* When xenon atoms are adsorbed in some confining space such as cages (clathrates) and one-dimensional channels, Xe NMR signals often demonstrate chemical shift anisotropy. Extensive experimental work done on ^{129}Xe NMR in clathrates and on a variety of one-dimensional channels as well as theoretical calculations have demonstrated the sensitivity of the ^{129}Xe shielding tensor to the shape, symmetry, size and chemical composition of the cages and channels in which the xenon is enclosed.[54,96,97] The major contribution to the interpretation of observed anisotropic NMR line shapes of xenon in nanochannels has been made in the recent years based on ab initio calculations of the ^{129}Xe shielding surfaces and Grand Canonical Monte Carlo.[57] The method has been successfully applied to different systems, and is capable to provide results reasonably close to the experimental observations.[33,54] In an ideal case of xenon atom absorbed in infinitely long nanochannels with a cylindrical cross-section at zero-loading limit, the shielding tensor is expected to be axially symmetric, with the components $\delta_{\parallel} \geq \delta_{\perp}$.

Effect of Channel Loading on the CSA. The theoretical work done by Jameson and co-workers and based on ab initio calculations has given useful guidelines to the behavior of the components of the shielding tensor with the channel loading.[54] In a diamagnetic narrow-bore pipe the anisotropy is expected to change as a function of channel loading from positive values at zero loading, where the component $\delta_{\perp}$ is the most shielded, to negative values at high loadings, where $\delta_{\perp}$ is the most deshielded. The component $\delta_{\parallel}$ remains unaffected by the filling of the channels. The expected trends are generally observed for all of the dipeptides studied. Our experimental data have also demonstrated a good sensitivity of the CSA to the loading of different channels. In situations where the xenon is in channels with a diameter smaller than its van der Waals diameter (VI, IV, IA, and VV, with channels ranging from 4.0 Å for VV to 3.0 Å for VI), a significantly greater positive anisotropy (∼100 ppm for VI at room temperature) characterizes the signals at high temperatures (low loading). The positive anisotropy is still observed even at the lowest temperature (high loading), although with its span reduced as compared to the high-temperature signal (an isotropic line shape is observed for VV at 173 K). This observation is consistent with very strong Xe−wall interactions in the narrow channels and with Xe−Xe interactions being unable to counteract these effects. For the narrowest channels, the Xe−Xe interactions could be also somewhat hampered by the geometry of the pores, which can be viewed as an alternation of wide and constricted volumes in a corrugated channel. This hypothesis is elaborated further below.

Effect of the Presence of Specific Sites on the CSA. Comparing to other dipeptides the CSA of Xe in the channels of LS, VI, and IV shows some distinctive features. At high temperature, all three show a linear behavior of each tensor component with decreasing temperature. In the narrowest channels of VI and IV, both the $\delta_{\parallel}$ and $\delta_{\perp}$ deshield linearly with decreasing temperature, whereas in LS, they become more shielded. Such a linear dependence of the ^{129}Xe chemical shift tensor components with average occupancy has been observed previously in molecular sieves ALPO-11[37] and SAPO-11[38] and ascribed to the presence of an ordered arrangement of xenon atoms within the channels driven by the existence of energetically favorable sites along the channel.[37]

It was recently pointed out that when these specific sites are too close to each other, linear behavior of the chemical shift tensor components is no longer observed.[56] It is interesting to note that the linear behavior is interrupted at some intermediate temperature for VI and IV and an exponential behavior similar to that observed for the dipeptides AV, VA, AI, VV, and IA is then observed at lower temperatures. This suggests that the structure of the channel may well have changed by the xenon absorbed, going from a corrugated to a smooth channel, where the Xe atoms have a chance to get closer to each other, similar to what observed in the larger channels.

Effect of Helicity and Diameter of the Channels on the CSA. To explain the influence of the helicity of the channels on the observed spectra, it is useful to consider again the ideal model of a single xenon atom in a straight nanochannel. In this case, the interactions between the absorbed xenon and the atoms constituting the cross-sectional plane of the channel are merely reflected in the parallel component $\delta_{\parallel}$ of the CSA tensor. On the other hand, interactions between an absorbed xenon atom and neighboring xenon atoms lying along the channel axis are mirrored in the perpendicular

(96) Ripmeester, J. A.; Ratcliffe, C. I.; Tse, J. S. *J. Chem. Soc., Faraday Trans.* **1988**, *84* (11), 3731–3745.
(97) Ripmeester, J. A. *J. Am. Chem. Soc.* **1982**, *104*, 289–290.

component $\delta_\perp$.[33,56] This ideal model suggests that the variation of the loading, which can be achieved by increasing the xenon pressure or decreasing the temperature, would cause a change in only $\delta_\perp$, leaving $\delta_\parallel$ unchanged.

The systems studied here, however, are more complicated than this ideal model. According to our experiments, $\delta_\parallel$ generally increases with decreasing temperature down to the lowest value achieved (173 K). It is worth noting, that $\delta_\parallel$ is practically constant for AI (see Figure 3b). According to helium pycnometry and crystallographic data,[8] AI channels have a diameter very close to the van der Waals diameter of xenon atoms and show very low helicity. The independence of $\delta_\parallel$ with the temperature complements the previous results suggesting that the xenon atoms absorbed inside the AI channels are aligned linearly along the channel axis. Calculations have demonstrated[55] that when angular arrangements of xenon atoms in highly loaded one-dimensional channels is characterized by angles in the range 180°−150° (i.e., linearly, to a good approximation) the component of the chemical shift tensor along the axis of the channel ($\delta_\parallel$) will hardly change with xenon occupancy. In helical channels, the effects of Xe−wall and Xe−Xe interactions are also spread out along the direction perpendicular to the axis of the channel. Consequently, the observed $\delta_\perp$ and $\delta_\parallel$ values are to some extent influenced when the temperature (and therefore the loading) is varied. Figure 2 suggests that, in fact, the Xe atoms absorbed in VA have angular positions with respect to each other considering the channel axis.

It is not straightforward, however, to directly correlate the helicity of the channels to the shielding of the parallel component. Most likely, the observed changes in $\delta_\parallel$ are both due to the variation in helicity and diameter of the channels. Channels with diameter larger than the xenon van der Waals diameter may allow zigzag alignment of xenon atoms in a channel even if the helicity of the channel is low.

Effect of Dynamics of Xe in the Cross-Section of the Pores on the CSA. Previous calculations based on Lennard−Jones potentials[26,27] and ab initio calculations,[54] suggest that when the xenon atoms are trapped in narrow pores having the same size as the xenon van der Waals diameter, they will remain along the center of the pipe. In the high-temperature region, however, where the zero-loading condition holds, increasing the temperature would result in a low field shift of δ_{iso}. This has been explained[54] by the effect of the Xe dynamics inside the nanopores on the components of the shielding tensor. Experimentally observed deshielding of $\delta_\parallel$ with increasing temperature is in agreement with that predicted by ab initio calculations.[54] This leads to an increase in the span and in δ_{iso}, the component $\delta_\perp$ being almost unaffected. In other words, at higher temperatures, the interactions between xenon atoms and the channel walls are more pronounced.[54] Overall, the effect is dependent on the diameter of the channel as discussed above. The aforementioned theoretical predictions, however, do not apply to the experimental results for the channels LS, IV, and VI which are too narrow to have a significant contribution from Xe motion.

Conclusions

This study exploits the continuous-flow HP ^{129}Xe NMR technique to extract comprehensive information on the thermodynamics and molecular-scale details of xenon sorption in a series of microporous dipeptides. The isosteric heats of sorption have been determined for each material for the high and low levels of loading of the solids with xenon. The introduced approach is based on the extraction of sorption isobars under the dynamic conditions imposed by the continuous-flow HP ^{129}Xe NMR experiments. Interaction of Xe with the porous space of dipeptides is analyzed with two independent methods based on the temperature dependence of (1) the intensities and (2) isotropic chemical shifts of the xenon NMR signal. The first method is applicable in the high-temperature region, where the loadings are close to zero. The second method applies to the low-temperature region, where the loading is close to maximum. Reasonable agreement between the isosteric heats of sorption derived by the two methods (the values are expected to be different but not by more than 20−30%) as well as reasonable trends in the values in the series studied confirm the validity of the thermodynamic model proposed and substantiate the characterization approach introduced. Until now, the isobaric measurements have been applied to nonporous materials,[30,60] and the approach demonstrated in this study may become a useful tool for evaluation of a wide range of porous materials.

As compared to traditional studies based on the determination of a series of sorption isotherms, the sorption isobar approach is much faster and may be used, as illustrated in this study, for characterization of less-stable materials or materials subjected to deterioration progressing in time. Also, the method is much more applicable to materials with very narrow pores when the equilibrium with the total bulk of the sorbent is not easy attainable. The possibility to cross-check the data obtained from signal intensities and from chemical shifts makes it possible to control the adequacy of measurements: the data extracted from the chemical shifts do not depend on the total amount of the sorbent, whereas the underestimation of this amount in a sorption isotherm measurement (for example, because of a nonporous impurity) could essentially ruin the results. High sensitivity of the method allows to work with very small amounts of materials, which could be as low as tens of milligrams. All available spectral information allows for comprehensive conclusions on the structural details of the microporous space and molecular-scale information on interaction of Xe with the channels of dipeptides. In particular, an estimate of the pore diameter is available and reasonable assumptions about the pore geometry can be made. A drawback of the method used is the lack of information on the absolute values of loading, that is, the absolute capacity of a sorbent. This information should be obtained from an independent experiment, i.e., from a single adsorption measurement or estimated from the crystal structure of the porous material. For the dipeptides in the present study, the capacity of AV and VA was calculated as 0.5 mol of Xe per mol of dipeptide,[14] whereas the values for the other studied materials, as estimated from their crystal structures,[8] should be in the range 0.33−0.5 mol of Xe per mol of dipeptide.

Previous works have illustrated the use of the continuous-flow HP ^{129}Xe NMR technique mostly for qualitative characterization of porous solids.[8,14,28,31] Recently continuous-flow NMR techniques on various nuclei were also used to study catalyzed chemical reactions in zeolites.[98–101] This study provides a precedent for the use of continuous-flow HP ^{129}Xe NMR measurements for a rapid and comprehensive description of sorption, providing both quantitative information on fundamental thermodynamic parameters and qualitative understanding of the structural changes and dynamics accompanying the process on the microlevel.

Abbreviations Used

AV, L-alanyl-L-valine
VA, L-valyl-L-alanine
AI, L-alanyl-L-isoleucine
VV, L-valyl-L-valine
IA, L-isoleucyl-L-alanine
IV, L-isoleucyl-L-valine
VI, L-valyl-L-isoleucine
LS, L-leucyl-L-serine
CF, continuous flow
HP, ^{129}Xe-hyperpolarized xenon
$D^{(He)}$, average diameter of the channel calculated from He pycnometry results;
K_L, Langmuir constant
k_{probe}, coefficient defining the volumes ratio for the gas and sorbent in the coil region of the probe;
K, equilibrium (sorption) constant defined by the ratio of activities of adsorbed and gas phase xenon;
k', temperature-independent portion of Langmuir constant
k_0, pre-exponential coefficient (temperature-independent entropy term)
Θ_{rel}, relative coverage defined as a fraction of maximal coverage
q_{st}, isosteric heat of sorption
$\Delta G°$, free energy of the sorption process defined by eq 1
$\Delta S°$, standard entropy of the sorption process defined by eq 1
I_{ch}, integral intensity of the ^{129}Xe NMR signal corresponding to xenon absorbed inside the channels
I_{gas}, integral intensity of the ^{129}Xe NMR signal corresponding to xenon in the gas phase
I, ratio I_{ch}/I_{gas}
δ_{obs}, observed ^{129}Xe NMR chemical shift
δ_0, ^{129}Xe NMR chemical shift of xenon gas at zero pressure, 0 by convention
δ_{Xe-Xe}, chemical shift relative to the contribution of Xe−Xe interactions between absorbed xenon atoms to the observed chemical shift
δ_M, chemical shift relative to the contribution of the presence of interactions between absorbed xenon paramagnetic species to the observed chemical shift
B_0, principal external magnetic field in an NMR experiment
B_1, local magnetic field caused by electrons surrounding the nucleus observed by NMR
B_{eff}, effective field experienced by the nucleus observed by NMR
CSA, chemical shift anisotropy
δ_{11}, δ_{22}, δ_{33}, principal components of the shielding tensor
$\Omega = \delta_{11} - \delta_{33}$, span of the CSA
$\kappa = 3(\delta_{22} + \delta_{iso})/\Omega$, skew of the CSA
$\delta_{iso} = (\delta_{11} + \delta_{22} + \delta_{33})/3$, isotropic chemical shift δ_s - ^{129}Xe NMR isotropic chemical shift defined by Xe-wall interactions only and corresponds to the shielding of a single xenon atom in the empty channel
δ_f, ^{129}Xe NMR isotropic chemical shift of xenon in completely filled channels
$\rho\delta$, ^{129}Xe NMR isotropic chemical shift corresponding to the difference $\delta_f - \delta_s$
Xe−Xe, interactions between absorbed xenon atoms
Xe−wall, interactions between absorbed xenon atoms and atoms constituting the channel walls.

Acknowledgment. D.V.S. thanks the Steacie Institute for Molecular Sciences for support.

Supporting Information Available: Continuous-flow HP ^{129}Xe NMR spectra of AV, LS, VV, IA, IV, and VI dipeptides in the 173−343 K temperature range;experimentally observed dependences ln(I) versus 1000/T for AV, VA, LS, AI, IV, and VI dipeptides and linear fits of the data in the high-temperature regions; experimentally observed room temperature ^{13}C CP MAS spectra of empty and Xe-loaded AV, VA, AI, LS, VV, IA, IV, and VI; summary of changes in ^{13}C chemical shifts of CH_3-groups in dipeptides upon absorption of Xe (PDF). This material is available free of charge via the Internet at http://pubs.acs.org.

CM8001805

(98) Wang, W.; Seiler, M.; Ivanova, I. I.; Sternberg, U.; Weitkamp, J.; Hunger, M. *J. Am. Chem. Soc.* **2002**, *124*, 7548–7554.
(99) Hunger, M. *Microporous Mesoporous Mater.* **2005**, *82*, 241–255.
(100) Hunger, M. *Chem. Ing. Tech.* **2007**, *79*, 781–793.
(101) Sundaramurthy, V.; Cognec, J.-P.; Thomas, K.; Knott, B.; Engelke, F.; Fernandez, C. *C.R. Chim.* **2006**, *9*, 459–465.